Journal of
Composites Science

MDPI

Article

Rapid Prediction and Parameter Evaluation of Process-Induced Deformation in L-Shape Structures Based on Feature Selection and Artificial Neural Networks

Qingchuan Liu, Xiaodong Wang *, Zhidong Guan and Zengshan Li

School of Aeronautic Science and Engineering, Beihang University, Beijing 100191, China; liuqingchuan1215@163.com (Q.L.); zdguan@buaa.edu.cn (Z.G.); zengshanli@buaa.edu.cn (Z.L.)
* Correspondence: wangxd819@163.com

Abstract: The process-induced deformation (PID) during the manufacturing of thermosetting composite materials can significantly compromise manufacturing precision. This paper introduces an innovative method that combines a finite element analysis (FEA), feature classification algorithms, and an Artificial Neural Network (ANN) framework to rapidly predict the PID of a typical L-shaped structure. Initially, a comprehensive range of parameters that influence PID are compiled in this research, followed by the generation of a dataset through FEA considering viscoelastic constitutive models, validated by experimental results. Influential parameters are classified using Random Forest and LASSO regression methods, with each parameter rated according to its impact on PID, delineating their varying degrees of importance. Subsequently, through a hyperparameter analysis, an ANN framework is developed to rapidly predict the PID, while also refining the assessment of the parameters' significance. This innovative approach achieves a computational time reduction of 98% with less than a 5% loss in accuracy, and highlights that under limited computational conditions, considering only a subset or all of the parameters—the peak temperature, corner angle, coefficient of chemical shrinkage, coefficient of thermal expansion, curing pressure, and E_1—minimizes accuracy loss. The study demonstrates that machine learning algorithms can effectively address the challenge of predicting composite material PID, providing valuable insights for practical manufacturing applications.

Keywords: process-induced deformation; finite element analysis; process simulation; ANN framework

Citation: Liu, Q.; Wang, X.; Guan, Z.; Li, Z. Rapid Prediction and Parameter Evaluation of Process-Induced Deformation in L-Shape Structures Based on Feature Selection and Artificial Neural Networks. *J. Compos. Sci.* **2024**, *8*, 455. https://doi.org/10.3390/jcs8110455

Academic Editor: Marco Di Sciuva

Received: 4 September 2024
Revised: 17 October 2024
Accepted: 31 October 2024
Published: 3 November 2024

1. Introduction

With the increasing application of carbon fiber-reinforced resin matrix composites (CRFPs) in aerospace, automotive, construction, and energy industries, the challenges of residual stress and structural deformation in the manufacturing process are growing prominent. This process-induced deformation (PID) can even lead to scrapped parts, resulting in high production costs. In early studies [1–3], the researchers spent a lot of effort to study the mechanism of part deformation during the curing process, thereby transforming the high-cost trial-and-error experiment optimization process into low-cost theoretical and numerical simulation methods [4,5]. The PIDs of L-shaped composite laminates have been investigated by numerous scholars [6–8]; introducing PID of structures with curvature is caused by different curing strains inside and outside the plane and structural design parameters, such as the curing temperature [9], layup sequence [10], corner angle [11], thickness [12], and tool–part interaction [13]. Incorporating all relevant parameters in PID calculations using FEA presents challenges such as extended computation times and convergence issues [14]. This highlights the inherent limitations of FEA methods in solving PID problems. A key challenge in engineering practice is selecting which parameter to prioritize to balance computational cost and accuracy [15]. Therefore, it is essential to rank the importance of these parameters.

With the rapid development of computer technology and artificial intelligence, machine learning (ML) can replace the traditional solution of many scientific research and engineering problems in an efficient method [16]. In the field of composite materials research, many scholars have successfully used machine learning methods to solve problems. The PID of asymmetric ply laminates was predicted by ANN, using the dataset calculated by FEM for training [17]. By using a decision tree regression model, the elastic modulus of individual fibers can be predicted based on the macroscopic modulus [18]. Recent studies have shown that smart sampling strategies, such as active learning and intelligent sampling, can significantly influence the predictive accuracy of machine learning models by efficiently utilizing data [19,20]. By selecting the most informative data points and applying a random number generator for each feature, defined by minimum and maximum values and a specified number of points within the interval or a step size, these strategies can reduce the required data volume and enhance model performance, which is particularly beneficial when dealing with limited or costly data acquisition. It is possible to divide the types of PID results of asymmetric composite laminates with different layup sequences, and realize the classification of curing results [21]. The potential influencing parameters of PID are numerous. In traditional analytical or numerical simulation methods, despite attempts to comprehensively account for all these parameters, there remain inherent limitations that cannot be entirely mitigated [15]. The feature selection algorithm can quantitatively obtain each parameter's influence degree of PID in order to distinguish the main parameters [22]. The directional influence degree and value range of each influencing parameter were discussed from the perspective of existing research findings and manufacturing experience.

In this paper, the input variables are reasonably selected or established according to theoretical knowledge, and this work proposes an appropriate machine learning algorithm to solve the problem of PID prediction. Firstly, all the parameters affecting the PID of an L-shaped structure are systematically analyzed. A finite element analysis (FEA) model is established based on summarized parameters. By setting random parameter values, the corresponding spring-in angle, referring to the geometric distortion that occurs during the curing process of composite parts particularly in curved sections, is obtained, and the acquisition of the dataset is completed. Based on the obtained dataset, preliminary feature selection is proposed through Random Forest Regression (RFR) and LASSO regression (LR), and the important, moderately important, and unimportant features are divided according to the relevance. In this study, an ANN framework was constructed, and the associated hyperparameters were identified and optimized. Training and predictive tasks were performed, leading to an adjustment of the feature classification outcomes. Furthermore, the influence of data volume and input characteristics on the predictive efficacy of the ANN was examined, with findings derived from various training datasets.

2. Analysis of Influential Parameters

This study summarizes and analyzes the parameters involved in the manufacturing of composite material structures, resulting in a determination of the parameter distribution range. All composite L-shaped structural influential parameters are shown in Figure 1. It can be mainly divided into external and internal parameters. External parameters include tool–part interaction and curing temperature, and internal parameters include L-shaped structural geometric parameters and material properties.

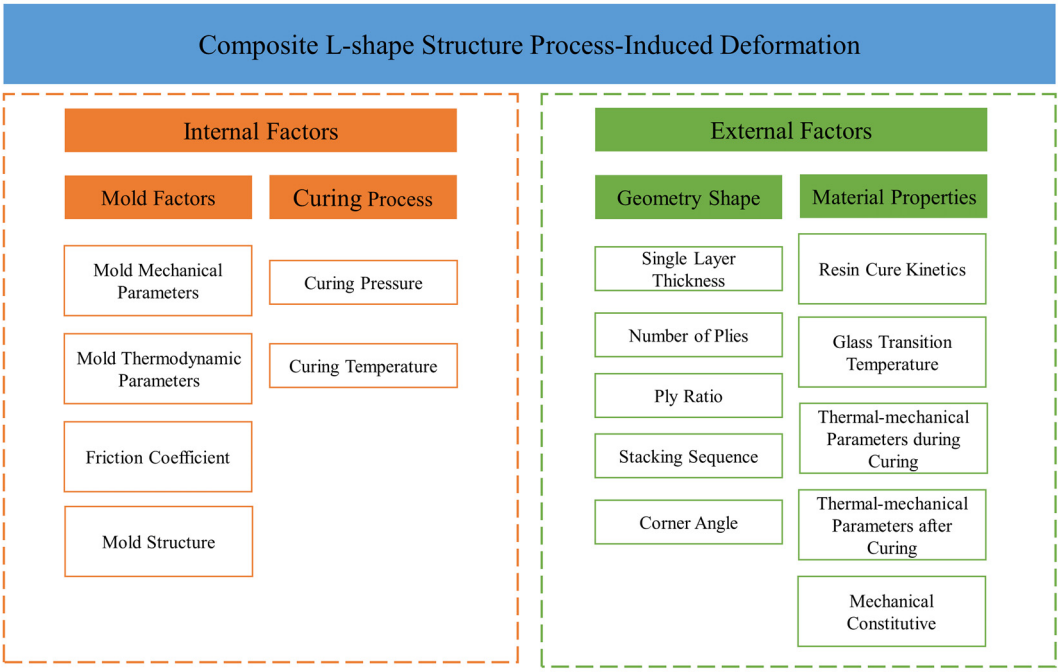

Figure 1. Influencing parameters of L-shape structure's PID.

2.1. Tool–Part Interaction

Tool–part interaction is determined by the thermal properties of the mold and the frictional effects. Thermal parameters of the tools refer to the coefficient of thermal expansion of the mold (CTE_{tool}). The materials of tools determine the CTE_{tool} and are usually an aluminum alloy [7] (23.6×10^{-6}), Q235 carbon steel [23] (12×10^{-6}), Invar [6] (1.5×10^{-6}), etc. Therefore, the range of CTE_{tool} is 1.5×10^{-6}~24×10^{-6}. The tool–part friction coefficient is usually obtained by the correction of the experiments and FEA, which cannot be ignored. According to the literature, the value was selected as 0~0.6 [4].

2.2. Curing Process Parameters

Cure pressure (P_{curing}) causes friction between the mold and the structure. In common processes, the values of P_{curing} are 0.6 MPa [24], 0.1 MPa [25], 0.689 MPa [26], etc., and the value range is set as 0.1~0.7 MPa. The previous research indicates that when the curing degree of the resin is small, the temperature change has little influence on the final curing deformation result [8]. Hence, it is more pertinent to concentrate on the analysis of peak temperature (T_{max}) in this research context. The common values of T_{max} are 450 K [27], 453 K [28], 448 K [24], 363 K [29], 373 K [30], 438 K [31], and 422 K [32], so the value range is 350 K~460 K.

2.3. Geometric Parameters

The thickness of the single layer and the number of layers are the parameters that determine the thickness of the composite structure, and the thickness will affect the spring-in angle, so it needs to be considered. The common thickness of composite material structure is about 1~20 mm, so the thickness of the single layer is usually taken as 0.1~0.2 mm, and the number of layers can be taken as 8~100.

The most common ply angle includes $[0/90/45/-45]$ plies. Other angles are rarely used, and these four angles are sufficient to cover the possible plies.

The ply ratio and stacking sequence affect the stiffness and residual stress distribution of the composite structure. The layer ratio is the proportion of each layer, including four parameters in total. The stacking sequence is not a continuous variable, so it is necessary to change the stacking sequence information into a continuous variable through

transformation. This transformation needs to fully reflect the stacking sequence information. In classical laminate theory, the stress–strain of a laminate is calculated by the laminate stiffness matrix:

$$\begin{bmatrix} N \\ M \end{bmatrix} = \begin{bmatrix} A & B \\ B & D \end{bmatrix} \begin{bmatrix} \varepsilon \\ \kappa \end{bmatrix} \tag{1}$$

This total matrix can be calculated using the material stiffness invariant U and 12 laminate parameters [33]:

$$\begin{bmatrix} A_{11} \\ A_{22} \\ A_{12} \\ A_{66} \\ A_{16} \\ A_{26} \end{bmatrix} = h \begin{bmatrix} 1 & \xi_1^A & \xi_2^A & 0 & 0 \\ 1 & -\xi_1^A & \xi_2^A & 0 & 0 \\ 0 & 0 & -\xi_2^A & 1 & 0 \\ 0 & 0 & -\xi_2^A & 0 & 1 \\ 0 & \frac{\xi_3^A}{2} & \xi_4^A & 0 & 0 \\ 0 & \frac{\xi_3^A}{2} & -\xi_4^A & 0 & 0 \end{bmatrix} \begin{bmatrix} U_1 \\ U_2 \\ U_3 \\ U_4 \\ U_5 \end{bmatrix} \tag{2}$$

$$\begin{bmatrix} B_{11} \\ B_{22} \\ B_{12} \\ B_{66} \\ B_{16} \\ B_{26} \end{bmatrix} = \frac{h^2}{4} \begin{bmatrix} 0 & \xi_1^B & \xi_2^B & 0 & 0 \\ 0 & -\xi_1^B & \xi_2^B & 0 & 0 \\ 0 & 0 & -\xi_2^B & 0 & 0 \\ 0 & 0 & -\xi_2^B & 0 & 0 \\ 0 & \frac{\xi_3^B}{2} & \xi_4^B & 0 & 0 \\ 0 & \frac{\xi_3^B}{2} & -\xi_4^B & 0 & 0 \end{bmatrix} \begin{bmatrix} U_1 \\ U_2 \\ U_3 \\ U_4 \\ U_5 \end{bmatrix} \tag{3}$$

$$\begin{bmatrix} D_{11} \\ D_{22} \\ D_{12} \\ D_{66} \\ D_{16} \\ D_{26} \end{bmatrix} = \frac{h^3}{12} \begin{bmatrix} 1 & \xi_1^D & \xi_2^D & 0 & 0 \\ 1 & -\xi_1^D & \xi_2^D & 0 & 0 \\ 0 & 0 & -\xi_2^D & 1 & 0 \\ 0 & 0 & -\xi_2^D & 0 & 1 \\ 0 & \frac{\xi_3^D}{2} & \xi_4^D & 0 & 0 \\ 0 & \frac{\xi_3^D}{2} & -\xi_4^D & 0 & 0 \end{bmatrix} \begin{bmatrix} U_1 \\ U_2 \\ U_3 \\ U_4 \\ U_5 \end{bmatrix} \tag{4}$$

The material stiffness invariant U and stiffness property Q are calculated by

$$\begin{bmatrix} U_1 \\ U_2 \\ U_3 \\ U_4 \\ U_5 \end{bmatrix} = \frac{1}{8} \begin{bmatrix} 3 & 2 & 3 & 4 \\ 4 & 0 & -4 & 0 \\ 1 & -2 & 1 & -4 \\ 1 & 6 & 1 & -4 \\ 1 & -2 & 1 & 4 \end{bmatrix} \begin{bmatrix} Q_{11} \\ Q_{12} \\ Q_{22} \\ Q_{66} \end{bmatrix} \tag{5}$$

$$\begin{cases} Q_{11} = E_{11}^2 / \left(E_{11} - E_{22} v_{12}^2\right) \\ Q_{22} = E_{11} E_{22} / \left(E_{11} - E_{22} v_{12}^2\right) \\ Q_{12} = v_{12} Q_{22} \\ Q_{66} = G_{12} \end{cases} \tag{6}$$

where E_{11} is the axial modulus of the single-layer plate, E_{22} is the transverse modulus of the single-layer plate, G_{12} is the shear modulus of the single-layer plate, and ν_{12} is the principal Poisson's ratio of the single-layer plate. These 12 laminate parameters are calculated by the following formula:

$$\begin{bmatrix} \xi_1^k \\ \xi_2^k \\ \xi_3^k \\ \xi_4^k \end{bmatrix} = \int_{-\frac{h}{2}}^{\frac{h}{2}} Z^k \begin{bmatrix} \cos 2\theta \\ \cos 4\theta \\ \sin 2\theta \\ \sin 4\theta \end{bmatrix} dz, k = A, B, D, \begin{cases} Z^A = 1/h \\ Z^B = 4\,z/h^2 \\ Z^D = 12\,z^2/h^3 \end{cases} \tag{7}$$

where θ denotes the ply direction at the z-position of the thickness (the origin of the z-direction coordinate is the mid-plane). Both the ply ratio and the stacking sequence can be

automatically calculated from the known plies, so their corresponding input variables are the specific ply settings.

The corner angle and corner radius are both geometrical parameters of composite structures, and previous studies have demonstrated that the corner angle has a certain influence on PID, while the corner radius has little effect [23,34]. Therefore, the value range of the corner angle is 10~170 degrees, and the influence of the corner radius is ignored.

2.4. Material Properties

The thermal parameters for a single layer in the curing process include *CTE* and the coefficient of chemical shrinkage (*CCS*). The *CTE* can be considered constant throughout the curing process [8,35]. Based on commonly used composite laminate parameters, the *CTE* of a single layer ranges from $\alpha_1 = -1 \times 10^{-6}$~$1 \times 10^{-5}$, $\alpha_2 = 1 \times 10^{-6}$~$1 \times 10^{-4}$ [17]. The *CCS* is also an important parameter to consider, and previous studies have obtained values of the single-layer chemical shrinkage as $\beta_1 = -167$, $\beta_2 = -8810$ [27]; and $\beta_1 = -800$, $\beta_2 = -16{,}000$ [36]. In this study, the range of the single-layer CCS is taken as ($\beta_1 = -800$~-100, $\beta_2 = -20{,}000$~-5000).

The mechanical parameters of a single layer after curing primarily have a significant impact during the cooling stage. There are five independent parameters, values ranging from E_1 = 10~260 GPa, E_2 = 1~20 GPa, G_{12} = 1~10 GPa, G_{23} = 1~10 GPa, and ν_{12} = 0.3~0.4 [17].

The selection of the mechanical constitutive relationship of a single-layer plate can impact the accuracy of the calculations. In accordance with prior research results, a simplified viscoelastic constitutive model considering stress relaxation was selected [37], where the viscoelastic parameters are based on epoxy resin system 3501-6 as a reference.

In conclusion, the ANN model in this study encompasses 29 input parameters with their respective ranges as partly indicated in Table 1. The broad ranges of the input variables increase the diversity of the training data, which helps the ANN model to generalize better and make accurate predictions across different conditions. However, it also requires the model to capture more complex relationships between variables, which we addressed by optimizing the network architecture and training parameters.

Table 1. Ranges of Input Parameters.

Parameters		Minimum	Maximum
CTE_{tool}		1.5×10^{-6}	24×10^{-6}
Tool–part interaction		0	0.6
P_{curing}		0.1 MPa	0.7 MPa
T_{max}		350 K	460 K
Single-layer thickness		0.1 mm	0.2 mm
Number of plies		8	100
Ply angle		0/90/±45	
Corner angle		10°	170°
Single layer	CCS_1	−800	−100
	CCS_2	−20,000	−5000
	E_1	10 GPa	260 GPa
	E_2	1 GPa	20 GPa
	G_{12}	1 GPa	10 GPa
	G_{23}	1 GPa	10 GPa
	ν_{12}	0.3	0.4
	CTE_1	-1×10^{-6}	1×10^{-6}
	CTE_2	1×10^{-6}	1×10^{-6}

3. Dataset Based on FE Simulation

This study utilizes ABAQUS 6.13 software to simulate the residual stress and PID of an L-shaped structure. Due to the limitations of shell elements in capturing the material behavior in the thickness direction, three-dimensional solid elements are adopted to model and calculate the PID of composite laminates [4]. In this study, the composite structure is

simulated using C3D20R second-order reduced-integration 3D solid elements, while the mold elements are modeled using C3D8R first-order linear reduced-integration 3D solid elements. The analysis step is a "Static, general" step, and after curing, the tool is removed using the "Model Change" feature to complete the demolding process. The material properties are implemented through user-defined subroutines UMAT and UEXPAN. The FEA model, as shown in Figure 2, is thus established.

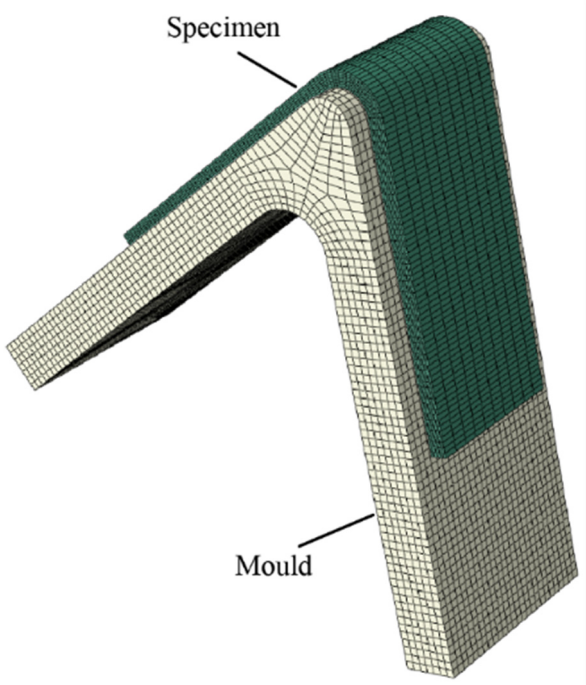

Figure 2. L-shape structure FE model.

The input parameters are randomly generated according to a uniform distribution. Owing to the significant number of iterations involved in FEA and the requirement for remeshing the model with newly generated random input parameters, a Python script was devised to automate the procedure of input parameter generation and simulation. Figure 3 illustrates the modeling process, specifying the relevant modeling content for the random input parameters. A total of 11,000 data samples were generated for the purpose of facilitating subsequent discussions.

The dimensions of the FEA model established in this study are consistent with the experimental setup described in the literature [38]. Furthermore, the FEA model used in this study was validated in a previously published paper [38] by other researchers from our research group.

The dimensions of the FEA and experimental models are shown in Figure 4. After comparing with other researchers' experimental results [6,39], apart from the $[90]_{24}$, where the actual spring-in deformation is minimal, making the error appear less precise, the deviation between the FEA data and experimental data is less than 10%, demonstrating that the dataset generated by the FEM is viable. The data are presented in Table 2. "Error" in Table 2 refers to the error compared to the experiment. For details regarding the input–output ranges and related discussion, please refer to Appendix A.

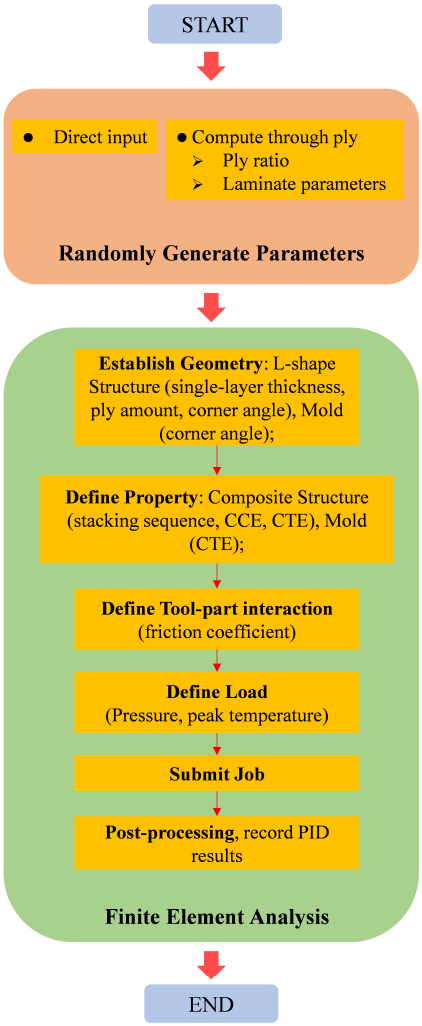

Figure 3. FEA model generation dataset process.

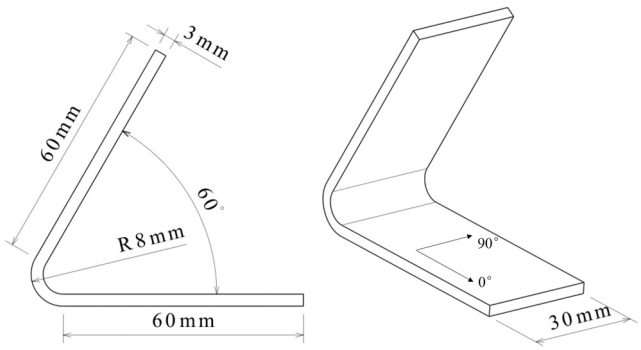

Figure 4. The dimensions of the FEA and experimental models.

Table 2. Comparison of curing spring-in angles between FEA and Experimental Data.

Part Number	Layup	Thickness (mm)	Corner Angle (°)	Δθ (°)			Error
				Exp	FEA	CHILE Model [39]	
1	$[0]_{24}$	3	60	1.37	1.29	1.71	5.84%
2	$[90]_{24}$	3	60	0.23	0.08	0.08	65.2%
3	$[45/90/-45/0]_{2s}$	2	60	1.84	2.08	2.40	7.61%
4	$[45/90/-45/0]_{3s}$	3	60	1.81	1.68	2.03	7.18%
5	$[45/90/-45/0]_{3s}$	3	90	1.32	1.39	1.64	5.30%

4. ANN Dataset Preprocessing

4.1. Data Normalization

Data normalization is necessary to eliminate the influence of dimensions between features before importing into an ANN. For the input parameters, the features have varying dimensions, which can affect their comparability. To mitigate this issue and ensure the consistency of the data, the input features are normalized to eliminate the influence of differing dimensions. As the output data consist solely of spring-in angles, which are directly comparable, normalization is applied exclusively to the input features. Commonly used normalization techniques include the min–max normalization method and the standardization method [21]. In this study, we employed the min–max normalization method for data preprocessing. Since our feature data were generated using Monte Carlo simulation with a uniform distribution, this method is appropriate for scaling the data effectively without being influenced by noise or outliers.

4.2. Feature Selection

Prior to training ANN, feature selection is beneficial in simplifying the model, reducing computational costs, and decreasing the risk of overfitting [18]. In this study, feature selection was performed to categorize numerous influencing parameters into important, moderately important, and unimportant features. The impact of these three types of features on model accuracy was investigated to obtain the optimal training scheme for comparing the number of input parameter types, input data quantity, and prediction accuracy. In machine learning, commonly used selection techniques include RFR and LASSO algorithms.

4.2.1. Regression Feature Selection of Random Forest

To investigate the influence of data quantity on RFR, different volumes of datasets were used as input data to complete selection, with the range of data group numbers from 1000 to 11,000. The process of RFR is shown in Figure 5. The data were randomly divided into a 70% training dataset and 30% testing dataset for training.

The results are further presented in a dot plot in Figure 6 to provide a more intuitive visualization of the feature importance. Several features, such as T_{max}, the corner angle, CCS_2, CTE_2, P_{curing}, and E_1, demonstrated large importance indicators, and were identified as important features in this study.

Although the importance values of certain features are relatively small, they still exhibit some degree of influence. For a dataset size of 11,000, we define features with importance values greater than or equal to 0.004 among the remaining features as 'moderately important features'. These include the CTE_{tool}, tool–part interaction, single-layer thickness, number of plies, 90° ply ratio, laminate parameter B2, CCS_1, E2, ν_{12}, G_{12}, G_{23}, and CTE_1. Features with minimal importance scores, which contribute negligibly to the prediction outcomes, are considered 'unimportant features'. These include the $0/45/-45$ ply ratio and laminate parameters A1, A2, A3, B1, B3, C1, C2, and C3. Overall, the feature selection analysis provided valuable insights into the relative importance of the features for predicting the target variable, and the results can guide the further optimization of the predictive models in this domain.

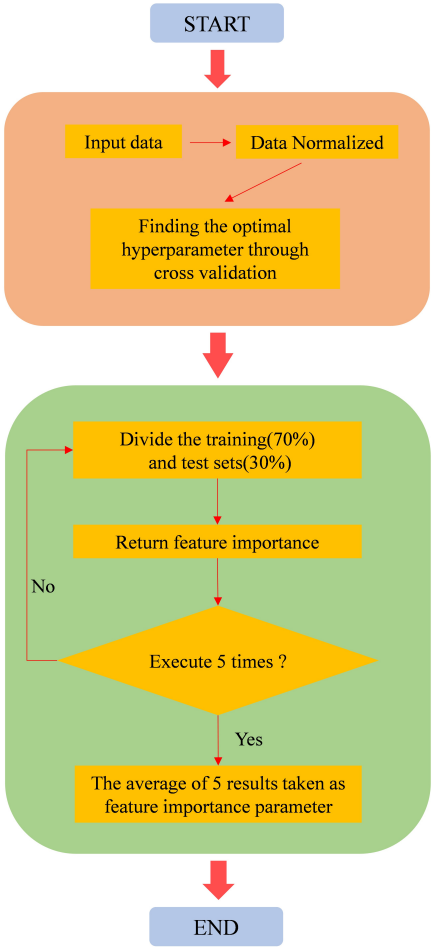

Figure 5. RFR feature selection process.

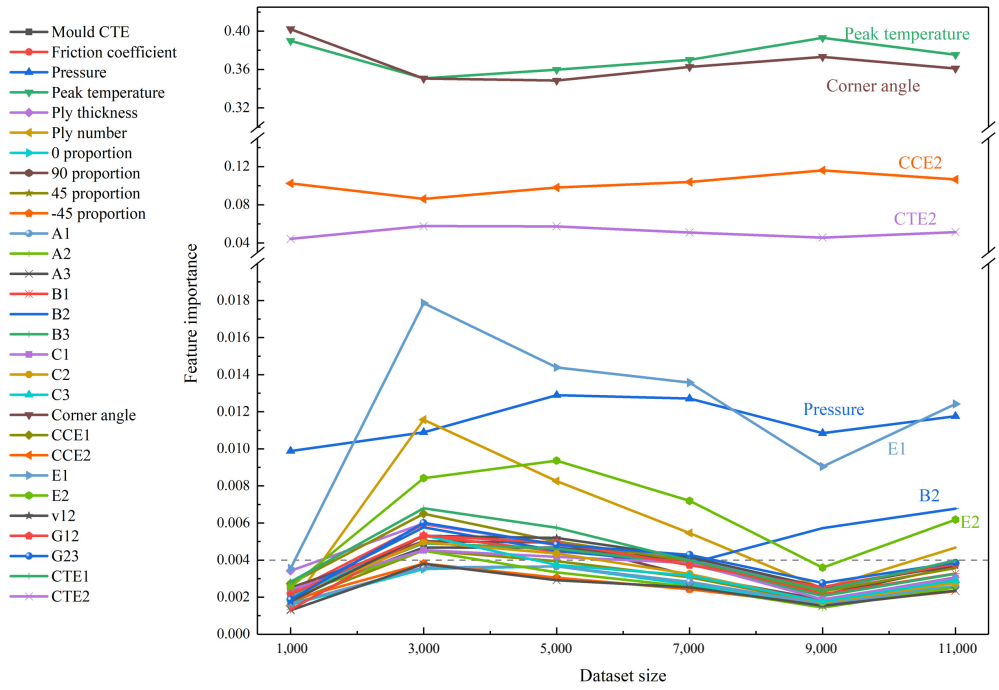

Figure 6. Results of RFR feature selection.

4.2.2. Lasso Regression Feature Selection

The Lasso (Least Absolute Shrinkage and Selection Operator) method is a compression estimation technique that operates on the principle of reducing the dataset (dimensionality reduction). It introduces an L1-norm penalty term in the loss function to prevent the coefficients of the feature variables from being too large and causing overfitting. The loss function of Lasso regression is given by

$$min\frac{1}{2n}\sum_{i=1}^{n}(\hat{y}_i - y_i)^2 + \lambda\sum_{j=1}^{k}|w_j| \quad (8)$$

In the given equations, n denotes the number of samples, $\hat{y}_i$ represents the predicted value of the i-th sample, y denotes the true value of the sample, k is the number of features, and w_j represents the coefficient of j. The parameter λ controls the degree of regularization in the loss function. It is essential to note that the sparsity matrix property resulting from L1-norm regularization allows for selection, which is a widely used technique in machine learning.

In order to investigate the impact of the amount of data on feature selection in LASSO, the dataset consisting of 1000–11,000 groups of input data was utilized. The process of LASSO is illustrated in Figure 7. The λ was selected and used for training to obtain the coefficients of each feature. For each λ, the dataset was randomly partitioned and trained five times, and the average value was taken as the feature coefficient result.

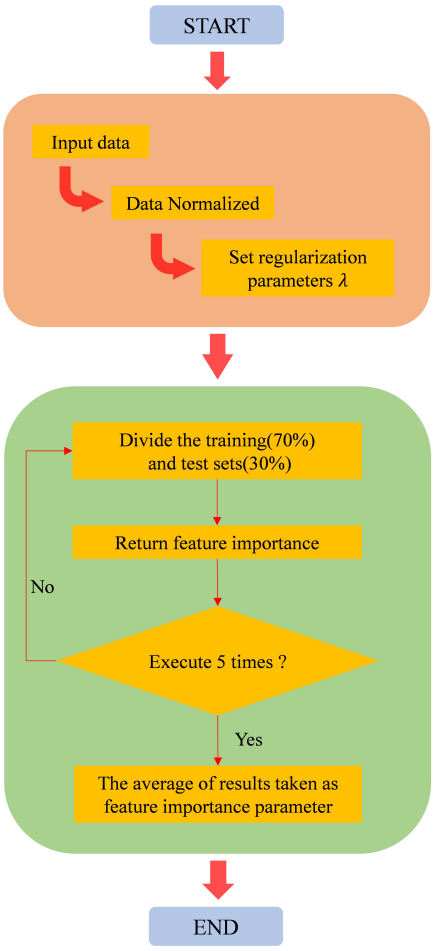

Figure 7. LASSO feature selection process.

After calculation, the feature classification results for different data volumes are shown in Table 3, where A represents important features, B represents moderately important features, and C represents unimportant features. The specific numerical values of the coefficients for each feature are affected by different data volumes, and the results tend to stabilize as the data volume increases. We take the result of the selection using LASSO with a data volume of 11,000 as a reference.

Table 3. Results of LASSO selection.

Parameters	Dataset Volume					
	1000	3000	5000	7000	9000	11,000
CTE_{tool}	B	B	B	C	C	B
Tool–part interaction	B	B	C	C	C	C
P_{curing}	A	A	A	A	A	A
T_{max}	A	A	A	A	A	A
Ply thickness	B	B	B	B	C	B
Ply number	B	B	B	B	B	B
0° proportion	B	C	B	B	C	C
90° proportion	C	C	C	C	B	B
45° proportion	C	C	C	C	C	C
−45° proportion	C	B	C	C	C	C
Parameter A1	C	C	B	B	B	B
Parameter A2	C	C	C	C	C	C
Parameter A3	B	B	C	C	C	C
Parameter B1	B	B	C	C	C	C
Parameter B2	B	C	B	C	B	B
Parameter B3	C	C	C	C	C	C
Parameter C1	B	C	C	C	C	C
Parameter C2	B	B	B	B	B	B
Parameter C3	C	C	C	C	C	C
Corner angle	A	A	A	A	A	A
CCS_1	B	B	B	B	B	B
CCS_2	A	A	A	A	A	A
E_1	A	B	B	B	B	B
E_2	B	B	B	B	B	B
v_{12}	B	C	B	C	C	B
G_{12}	B	B	B	B	B	B
G_{23}	A	B	B	B	B	B
CTE_1	B	B	B	B	B	B
CTE_2	A	A	A	A	A	A

4.2.3. Feature Classification Results

Both the RFR algorithm and LASSO algorithm can obtain the importance indicators of features, and have certain dependencies on data volume. The results of RFR and LASSO algorithms are mostly consistent, with some differences in the classification of certain features. Combining with a theoretical analysis, a reasonable classification is finally determined. The results obtained in this study are consistent with those derived from theoretical and experimental methods reported in the literature [40].

For important features, the common results of the two algorithms are T_{max}, the corner angle, CCS_2, CTE_2, and P_{curing}. In the RFR algorithm, E_1 is considered to have a greater importance. Theoretically, E_1 mainly determines the bending stiffness of the L-shaped structure. As analyzed in the previous text, when considering the frictional effect, the structural bending stiffness will affect the final rebound deformation result. Therefore, E_1 should be regarded as an important parameter. The T_{max} dictates the magnitude of cooling, which directly influences the thermal stress during the curing process and consequently contributes to deformation. The corner angle significantly affects the initial geometric configuration and is a critical factor in determining the curing spring-in behavior; for instance, if the angle increases to 180 degrees, the structure transforms into a flat plate,

and no internal stress would develop in symmetrically balanced laminates. The CCS_2 and CTE_2 govern the differential shrinkage between the in-plane and out-of-plane surfaces of the L-shaped structure, serving as the primary drivers of PID. Additionally, the P_{curing} determines the extent of interaction between the tool and the L-shaped structure, introducing shear effects that influence the magnitude of the spring-in angle. These factors, from a theoretical standpoint, represent the key influences on the spring-in deformation in L-shaped structures.

For moderately important features, the common results of the two algorithms are CTE_{tool}, single layer thickness, the number of layers, B2 of layer composite board parameters, CCS_1, E_2, v_{12}, G_{12}, G_{23}, and CTE_1. LASSO considers 90-degree layer proportion, A1 of layer composite board parameters, and C2 of layer composite board parameters as moderately important features. All these are considered as moderately important in this paper.

For unimportant features, their impact on PID can be neglected. That is, most of the layer proportion information and layer sequence information have little impact on PID. In summary, the classification results are shown in Table 4.

Table 4. Results of feature classification.

Categorization	Features	Amount
Important	T_{max}, corner angle, CCS_2, CTE_2, P_{curing}, E_1	6
Moderately Important	CTE_{tool} , tool–part interaction, single-layer thickness, number of plies, 90° ply ratio, laminate parameter A1, B2, C2, CCS_1, E2, v_{12}, G_{12}, G_{23}, CTE_1	14
Unimportant	0/45/−45 ply ratio, laminate parameter A2, A3, B1, B3, C1, C3	9

5. ANN Framework

The ANN mainly refers to several parameters. In this study, the key parameters of the ANN were determined by referring to the research results of other scholars [17] and by using the method of controlling variables. This study employed a neural network with a dropout rate of 0.5, which effectively alleviates overfitting and enhances model robustness, and also explored other techniques, such as a weight penalty and batch normalization, but found dropout to be the most effective.

In this study, the loss function was chosen as Mean Squared Error (MSE), with mean absolute error (MAE) and r^2 used as evaluation metrics.

5.1. Hidden Layer

Initially, we compared the results of a single hidden layer and a two-hidden-layer network, each with 100 fully connected neurons per layer, using the most important and second most important features as input. The dataset consisted of 7000 samples, and the results are shown in Figure 8. It can be seen that for our research case, the two-hidden-layer network is still too complex, resulting in severe overfitting and lower accuracy compared to the single-hidden-layer network. Therefore, we chose the single-hidden-layer network as our research model. The remaining overfitting phenomenon will be further addressed later in the paper.

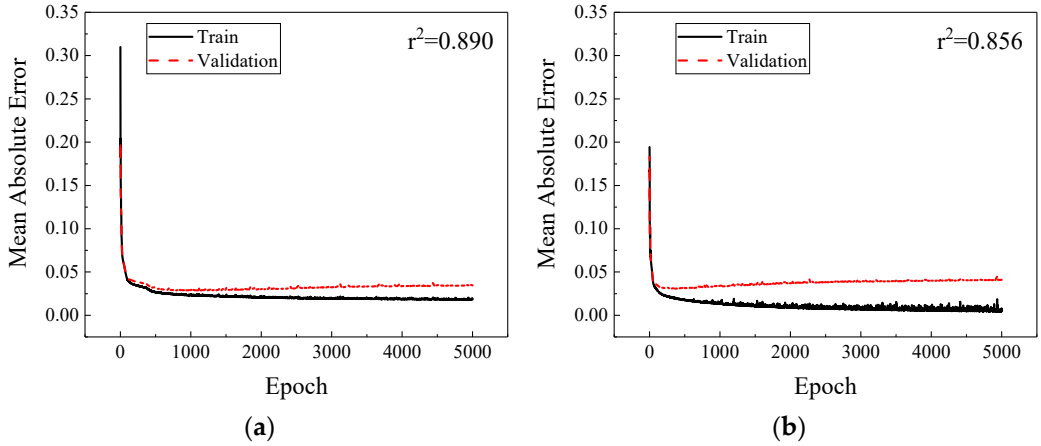

Figure 8. Results of different hidden layers. (**a**) Single hidden layer; (**b**) 2 hidden layers.

5.2. Number of Neurons

To select an appropriate number of neurons, a single-layer ANN model with a neuron range of 5–75 was established, with the same settings as above. The results are shown in Figure 9, the line refers to r^2. It can be seen that due to the simplicity of the data, the most suitable number of neurons is around 10. When the number of neurons is larger, the complexity of the model increases, leading to overfitting and a decrease in accuracy. When the number of neurons is smaller, the overfitting phenomenon is almost non-existent, but the predictive ability of the model is low, resulting in decreased accuracy. Therefore, this study selected 10 neurons as the ANN model parameter.

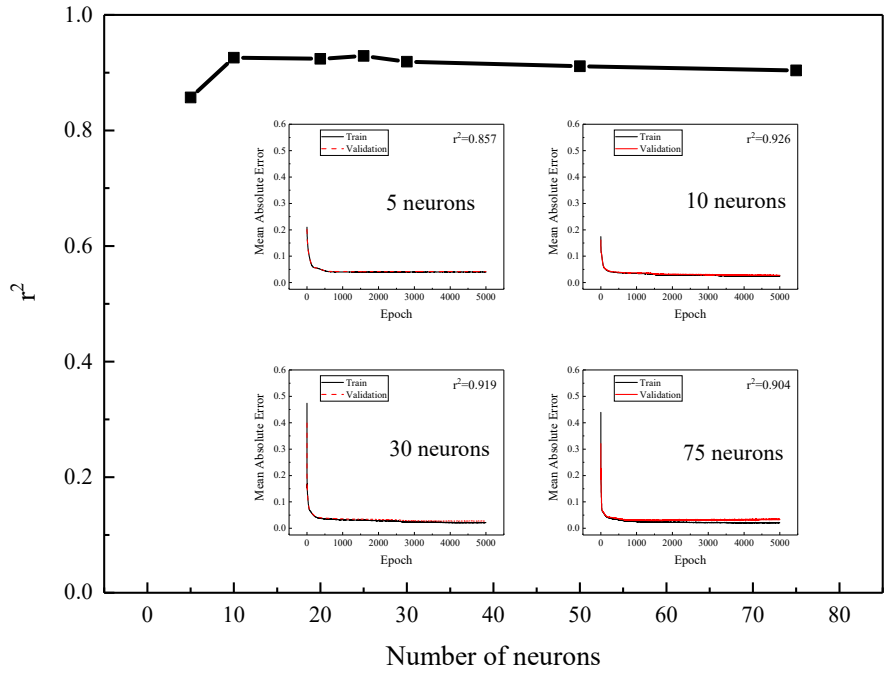

Figure 9. Results of the number of different neurons.

5.3. Activation Function and Optimizer

In this study, the linear activation function was chosen for the output layer, while the hidden layer was selected from the four types mentioned above. The calculation results are shown in Figure 10. It can be seen that except for the linear activation function, the other three activation functions have little effect on the results. Based on the results, this study selected ReLU as the activation function for the ANN model.

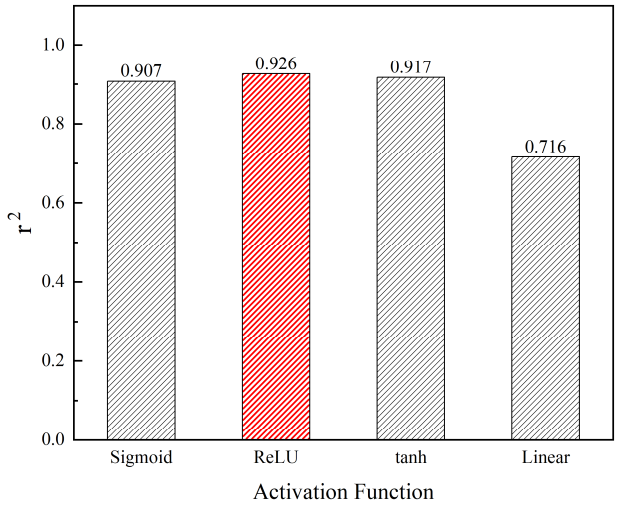

Figure 10. Results of activation function.

Considering the complexity and generalization requirements of the model in this study, using the controlled variable method, the most suitable optimizer was selected from the above optimizers. The compared results of optimizers are shown in Figure 11. Based on the results, this study selected Adam as the ANN model optimizer.

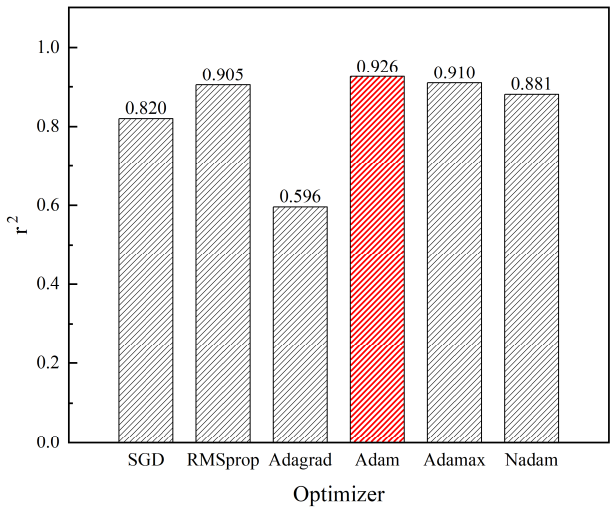

Figure 11. Results of optimizer.

The final ANN consists of one hidden layer with 10 neurons. ReLU was selected as the activation function for the hidden layer and the linear activation function was selected for the output layer. The Adam optimizer was chosen as the optimization algorithm for the model. The schematic diagram of the ANN architecture is illustrated in Figure 12.

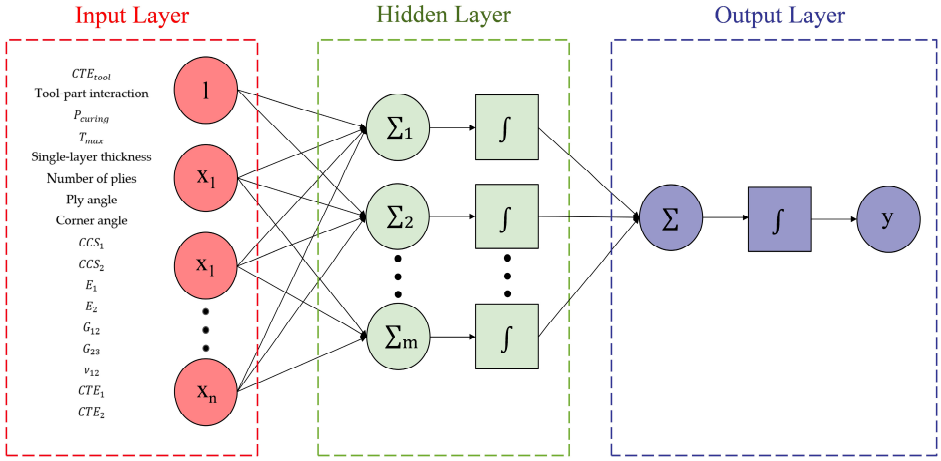

Figure 12. ANN framework.

6. Results and Discussion

6.1. Feature Analysis

In the previous section, feature selection was performed to classify all input features into three categories. However, the classification of some of the less important features was not entirely accurate. To further classify useful and useless features within the moderately important features, this study employed the previously optimized architecture to ensure accuracy. A model was trained and tested using only the important features as a benchmark. Subsequently, each moderately important feature was added to the important features as a shared input, and the accuracy of the training and prediction for each combination was evaluated. The results of this analysis, based on a data volume of 5000, are shown in Figure 13. The prediction accuracy using only the important features was 0.968. However, the inclusion of the 90° layup ratio, laminate parameter C2, and material property parameter E2 significantly improved the accuracy of the results and reduced the random fluctuations in the results. Therefore, these three features were retained as moderately important features. The introduction of other features decreased the accuracy of the results and was considered as noise. In this section, the importance of individual features was assessed by incrementally combining each feature with feature A, resulting in the formation of new feature groups. The impact of different groupings (A/A + B/A + B + C) on prediction accuracy will be discussed in detail in Section 6.2.1.

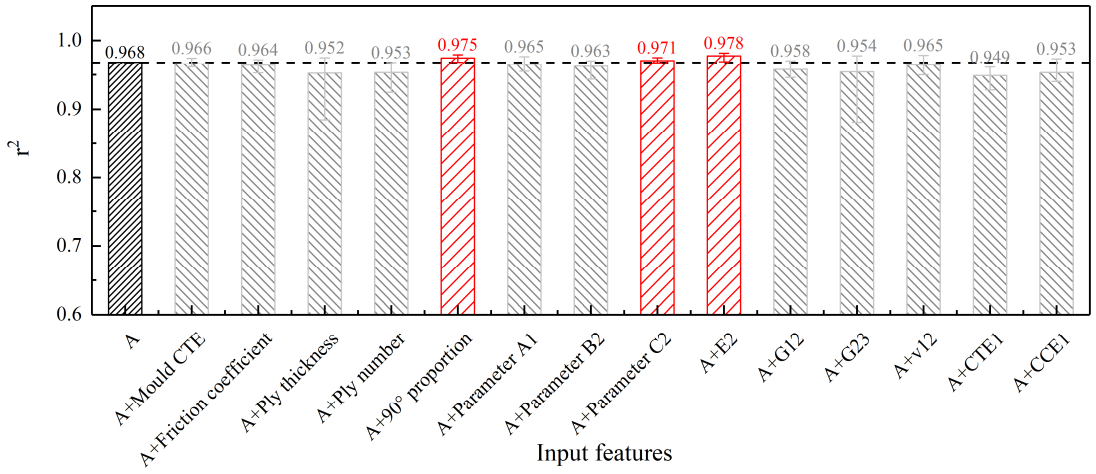

Figure 13. Further division of moderately important features.

In summary, only the 90° ply angle ratio, the C2 laminate parameter, and the E_2 were classified as moderately important. The reclassified features are shown in Table 5. When

the data volume was 5000, the accuracy increased to 0.979 when using important features with moderately important features.

Table 5. Recategorization of Feature Parameters.

Categorization	Features	Amount
Important	T_{max}, corner angle, CCS_2, CTE_2, P_{curing}, E_1	6
Moderately Important	90° ply ratio, laminate parameter C2, E2	3
Unimportant	CTE_{tool}, tool–part friction, single-layer thickness, number of plies, $0/45/-45$ ply ratio, laminate parameter A1, B2, A2, A3, B1, B3, C1, C3, ν_{12}, G_{12}, G_{23}, CTE_1, CCS_1	20

6.2. Influence of Data Volume and Input Features of ANN

Based on the redefined feature categories, the influence of data volume and input features on the accuracy of the ANN model's prediction results was studied. Training was conducted using three different input features, namely, A, A + B, and A + B + C, at different data volumes ranging from 200 to 8000 input data values. During training, 60% of the data were used for training, 20% for validation, and 20% for testing. To avoid the impact of randomness, each training was conducted five times, and the average value was taken as the final result. The analysis was conducted from three aspects, namely prediction accuracy, learning curves, and computational time.

6.2.1. Predictive Accuracy

The average predictive accuracy and fluctuation of further partitioning of the secondary features across different data volumes and input characteristics are depicted in Figure 14.

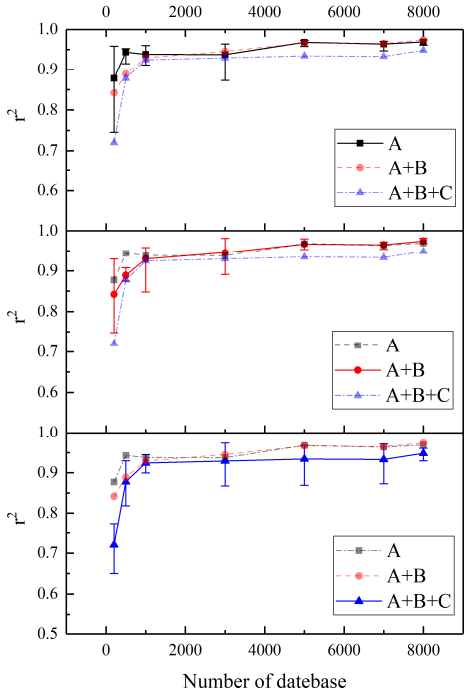

Figure 14. The predictive accuracy across varying data volumes and input features.

When the input feature is A (important), the model's prediction accuracy can reach a relatively high level with a small amount of data, indicating that the selected important

feature is indeed the main information determining the L-shaped structure rebound deformation. Additionally, with fewer inputs, the required training data are also relatively small. The accuracy stabilizes above 0.90 when the data volume reaches around 1000, and eventually stabilizes at around 0.96. This suggests that accurate models can be obtained with relatively small amounts of data when there are a small number of important input features.

When the input features are A + B (important and moderately important features), compared with the case where the input is only A, the dependence on the data volume increases due to the addition of more input. The prediction accuracy is lower than that of the case where the input feature is only A when the data volume is less than 1000. However, as the data volume continues to increase, its accuracy gradually increases, and eventually exceeds that of the case where the input is only A, stabilizing at around 0.97. The introduction of the secondary important feature improves the model's accuracy, but in this case, the data volume requirement is higher.

When the input features are A + B + C (important, moderately important, and unimportant features), compared with the previous two cases, an irrelevant feature is introduced, which not only increases the dependence on the data volume but also reduces the model's prediction accuracy, stabilizing at around 0.94 even with a large amount of data. This suggests that introducing irrelevant features may decrease the model's prediction accuracy and increase its fluctuation.

Overall, in terms of data volume, the results show that the accuracy of the model's prediction results continues to improve as the input data volume increases, and the fluctuation gradually decreases, particularly when the data volume is small. The accuracy improvement is not significant when the data volume is large, and the accuracy stabilizes at a certain value. Regarding the input, important features can already achieve high prediction accuracy, and the addition of moderately important features can further improve accuracy, although the improvement is small. However, introducing irrelevant features can reduce the accuracy of the model's prediction results and increase its fluctuation.

6.2.2. Learning Curves

The learning curves for different data volumes and input features are shown in Figure 15. The figure illustrates the training and validation mean absolute error (MAE) curves for the cases where the input is A, A + B, and A + B + C, respectively, and the corresponding data volumes are 200, 1000, and 5000, respectively. The iteration number for all cases is set to 5000. It can be observed that for all three cases, the training and validation curves diverge significantly when the data volume is small, indicating the occurrence of prediction errors, which becomes more severe as the number of inputs increases. This is because the ANN model has poor self-correcting ability during training when the data volume is small, i.e., the amount of information provided by the data is insufficient. When the data volume becomes sufficiently large, the model contains enough data information and the two curves tend to converge. Moreover, the comparison of different input features reveals that the model always converges faster when the number of inputs is small, which indicates that a smaller number of input features requires fewer iterations.

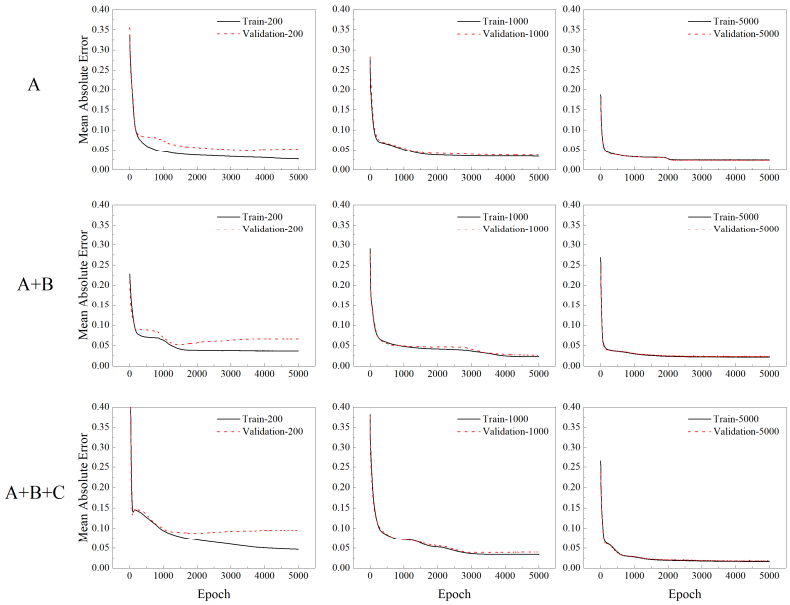

Figure 15. Learning curves for different data volumes and input characteristics.

6.2.3. Computation Time

The average computation time for each model, based on different data volumes and input features, is shown in Figure 16, using an i5-7200U CPU with 16 GB of memory, and simultaneously using an NVIDIA 2060s GPU with 8 GB of memory for accelerated training. The results indicate that computation time increases almost linearly with data volume. Additionally, increasing the number of input features also leads to longer computation times, but the increase is relatively small. Therefore, the primary parameter affecting computation time is the data volume.

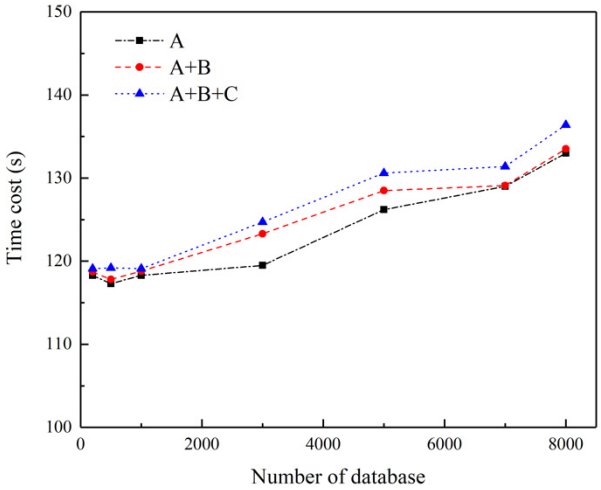

Figure 16. Computation time for different data volumes and input features.

7. Conclusions

In this paper, an ANN is constructed to predict the spring-in deformation of L-shaped composite structures. Utilizing a finite element analysis that incorporates a viscoelastic constitutive model, the dataset is generated, and an initial classification of features is carried out using RFR and LASSO algorithms. Subsequently, the ANN framework is employed to finalize the feature classification. The study also examines the effects of data volume and input features on the predictive accuracy of the ANN. The main conclusions of the study are detailed as follows:

- Using FEA and script generation, a dataset of spring-in deformation for an L-shaped structure was obtained, accounting for various parameters. Through the application of classification algorithms, it was determined that the parameters with the most significant impact on the PID analysis are T_{max}, the corner angle, CCS_2, CTE_2, P_{curing}, and E_1. Therefore, prioritizing these parameters in the analysis is crucial.
- A fundamental ANN framework, comprising a single hidden layer with 10 neurons, achieves a predictive accuracy of at least 95% in forecasting the PID of L-shaped structures. This performance suggests that the underlying dynamics of each influencing parameter are relatively straightforward. Moreover, as the volume of data increases, the predictive accuracy of the model correspondingly rises while variance diminishes. This enhancement is particularly notable in smaller datasets and tends to stabilize once the dataset size reaches a critical threshold.
- Given the constraint of limited input parameters, utilizing only the important features identified in the previous analysis ensures that the predictive model achieves the highest possible accuracy. This strategy helps maintain model precision while reducing the risk of accuracy loss associated with a smaller feature set.
- The primary parameter affecting computation time is data volume. With an increase in data volume, the computation time almost exhibits a linear growth trend. Moreover, an increase in input features also leads to an increase in computation time, albeit to a lesser extent.
- Machine learning methods can be effectively applied to simulate the PID of composite structures, thereby reducing the reliance on multi-physics coupling processes in FEA. This approach not only conserves significant computational resources but also enhances the efficiency of the analysis. The method we have validated is expected to be applicable to a broader range of resin formulations and composite materials.

Author Contributions: Conceptualization, Q.L. and X.W.; methodology, Q.L.; software, X.W.; validation, Q.L., X.W. and Z.G.; formal analysis, Z.L.; investigation, Q.L.; resources, X.W.; data curation, X.W.; writing—original draft preparation, Q.L.; writing—review and editing, X.W.; visualization, Z.L.; supervision, Z.G.; project administration, Z.G.; funding acquisition, X.W. All authors have read and agreed to the published version of the manuscript.

Funding: This research was funded by the National Key Research and Development Program of China, grant number 2021YFB3401700; Young Elite Scientists Sponsorship Program by CAST, grant number 2021QNRC001; and Aeronautical Science Foundation of China, grant number 2022Z039051001.

Data Availability Statement: The raw data supporting the conclusions of this article will be made available by the authors on request.

Conflicts of Interest: The authors declare no conflicts of interest.

Appendix A

The input–output ranges are presented as shown in Table A1. By using a uniform distribution for generating the input parameters within their specified ranges, we ensured an even and unbiased sampling across the entire parameter space. This approach allows the ANN model to learn from a comprehensive dataset that represents all possible combinations within the practical limits of the variables. The ranges were selected based on industry standards and the relevant literature to encompass the typical operating conditions for the resins and composites studied.

Table A1. Input–output Ranges.

	Max	Min
E_1	259,994	10,018
E_2	19,999	1007
ν_{12}	0.393	0.3
G_{12}	10,000	1001
G_{23}	9998	1000
CTE_1	1.00×10^{-5}	-1.00×10^{-6}
CTE_2	1.00×10^{-4}	1.01×10^{-6}
CCS_1	−102	−799
CCS_2	−4997	−19,998
0° ply percent	0.965304	2.54×10^{-5}
45° ply percent	0.98	1.13×10^{-4}
90° ply percent	0.98	2.24×10^{-4}
T_{max}	459.9	350.9
Corner angle	169.9	10
Thickness	0.19	0.11
$\Delta\theta$ (°)	1.65	−1.3

Below are some examples of resin formulations with glass transition temperatures (Tg) ranging between 350 K (77 °C) and 460 K (187 °C):

1. Epoxy Resins: By modifying standard epoxy systems with additives such as butyl glycidyl ether, the Tg can be reduced. For example, adding this modifier in various weight percentages (up to 20 wt%) to a diglycidyl ether of bisphenol A (DGEBA) and methylene dianiline (MDA) resin system resulted in a significant decrease in Tg, making it more suitable for applications requiring lower-temperature flexibility [41].
2. Bio-Based Epoxy Resins: Research has developed bio-based epoxy resins that utilize l-arginine as a curing agent. These formulations, such as Argopox-1 and Argopox-2.5, have demonstrated a Tg around 100 °C. The formulations are designed for applications in fiber-reinforced composites, where low viscosity and latency are crucial for processing [42].
3. Polyester and Polyurethane Resins: These resins can have Tg values ranging from 30 °C to 80 °C. They are suitable for adhesives and coating materials, offering good moldability and phase separation characteristics [43].

References

1. Hahn, H.T.; Pagano, N.J. Curing Stresses in Composite Laminates. *J. Compos. Mater.* **1975**, *9*, 91–106. [CrossRef]
2. Loos, A.C.; Springer, G.S. Curing of Epoxy Matrix Composites. *J. Compos. Mater.* **1983**, *17*, 135–169. [CrossRef]
3. Bogetti, T.A.; Gillespie, J.W. Process-Induced Stress and Deformation in Thick-Section Thermoset Composite Laminates. *J. Compos. Mater.* **1992**, *26*, 626–660. [CrossRef]
4. Zeng, X.; Raghavan, J. Role of Tool-Part Interaction in Process-Induced Warpage of Autoclave-Manufactured Composite Structures. *Compos. Part A Appl. Sci. Manuf.* **2010**, *41*, 1174–1183. [CrossRef]
5. Koteshwara, M.P. *Parametric Study of Process-Induced Warpage in Composite Laminates*; University of Manitoba: Winnipeg, MB, Canada, 2002.
6. Kappel, E.; Stefaniak, D.; Hühne, C. Process Distortions in Prepreg Manufacturing—An Experimental Study on CFRP L-Profiles. *Compos. Struct.* **2013**, *106*, 615–625. [CrossRef]
7. Sun, L.; Wang, J.; Ni, A.; Li, S.; Ding, A. Modelling and Experiment of Process-Induced Distortions in Unsymmetrical Laminate Plates. *Compos. Struct.* **2017**, *182*, 524–532. [CrossRef]
8. Liu, C.; Shi, Y. A Thermo-Viscoelastic Analytical Model for Residual Stresses and Spring-in Angles of Multilayered Thin-Walled Curved Composite Parts. *Thin-Walled Struct.* **2020**, *152*, 106758. [CrossRef]
9. Sarrazin, H.; Kim, B.; Ahn, S.-H.; Springer, G.S. Effects of Processing Temperature and Layup on Springback. *J. Compos. Mater.* **1995**, *29*, 1278–1294. [CrossRef]
10. Abdelal, G.F.; Robotham, A.; Cantwell, W. Autoclave Cure Simulation of Composite Structures Applying Implicit and Explicit FE Techniques. *Int. J. Mech. Mater. Des.* **2013**, *9*, 55–63. [CrossRef]
11. Salomi, A.; Garstka, T.; Potter, K.; Greco, A.; Maffezzoli, A. Spring-in Angle as Molding Distortion for Thermoplastic Matrix Composite. *Compos. Sci. Technol.* **2008**, *68*, 3047–3054. [CrossRef]

12. Wisnom, M.R.; Potter, K.D.; Ersoy, N. Shear-Lag Analysis of the Effect of Thickness on Spring-in of Curved Composites. *J. Compos. Mater.* **2006**, *41*, 1311–1324. [CrossRef]
13. Fiorina, M.; Seman, A.; Castanie, B.; Ali, K.M.; Schwob, C.; Mezeix, L. Spring-in Prediction for Carbon/Epoxy Aerospace Composite Structure. *Compos. Struct.* **2017**, *168*, 739–745. [CrossRef]
14. Chaln Chavez, A.M.; Guevara Paredes, K.E. Process Modelling for Distortions in Manufacturing of Fibre Reinforced Composite Materials. Master's Thesis, Boğaziçi Üniversitesi, Istanbul, Turkey, 2014.
15. Bellini, C.; Sorrentino, L.; Polini, W.; Corrado, A. Spring-in Analysis of CFRP Thin Laminates: Numerical and Experimental Results. *Compos. Struct.* **2017**, *173*, 17–24. [CrossRef]
16. Carlone, P.; Aleksendrić, D.; Ćirović, V.; Palazzo, G.S. Meta-Modeling of the Curing Process of Thermoset Matrix Composites by Means of a FEM-ANN Approach. *Compos. Part B Eng.* **2014**, *67*, 441–448. [CrossRef]
17. Luo, L.; Zhang, B.; Zhang, G.; Li, X.; Fang, X.; Li, W.; Zhang, Z. Rapid Prediction and Inverse Design of Distortion Behaviors of Composite Materials Using Artificial Neural Networks. *Polym. Adv. Technol.* **2021**, *32*, 1049–1060. [CrossRef]
18. Qi, Z.; Zhang, N.; Liu, Y.; Chen, W. Prediction of Mechanical Properties of Carbon Fiber Based on Cross-Scale FEM and Machine Learning. *Compos. Struct.* **2019**, *212*, 199–206. [CrossRef]
19. Couto, C. Neural Network Models for the Critical Bending Moment of Uniform and Tapered Beams. *Structures* **2022**, *41*, 1746–1762. [CrossRef]
20. Zhou, C.; Xie, Y.; Wang, W.; Zheng, Y. Machine Learning Driven Post-Impact Damage State Prediction for Performance-Based Crashworthiness Design of Bridge Piers. *Eng. Struct.* **2023**, *292*, 116539. [CrossRef]
21. Luo, L.; Zhang, B.; Zhang, G.; Xu, Y. Rapid Prediction of Cured Shape Types of Composite Laminates Using a FEM-ANN Method. *Compos. Struct.* **2020**, *238*, 111980. [CrossRef]
22. Pereira, G.C.; Yoshida, M.I.; LeBoulluec, P.; Lu, W.T.; Alves, A.P.; Avila, A.F. Application of Artificial Intelligence Models for Predicting Time-Dependent Spring-Back Effect: The L-Shape Case Study. *Compos. Sci. Technol.* **2020**, *199*, 108251. [CrossRef]
23. Wang, Q.; Guan, Z.; Wang, R.; Nie, H.; Jiang, T. Numerical Simulation on Process-Induced Deformation of Autoclaved V-Shaped Composite Parts. In Proceedings of the 2016 7th International Conference on Mechanical and Aerospace Engineering (ICMAE), London, UK, 18–20 July 2016; pp. 23–28. [CrossRef]
24. Hardiman, M.; Vaughan, T.J.; McCarthy, C.T. The Effect of Microscale Residual Stress from Thermal Cooldown on the Nanoindentation Properties of Fibre-Reinforced Composites. *J. Compos. Mater.* **2016**, *50*, 4147–4158. [CrossRef]
25. Sun, J.; Gu, Y.; Li, Y.; Li, M.; Zhang, Z. Role of Tool-Part Interaction in Consolidation of L-Shaped Laminates during Autoclave Process. *Appl. Compos. Mater.* **2012**, *19*, 583–597. [CrossRef]
26. Li, D.; Li, X.; Dai, J.; Xi, S. A Comparison of Curing Process-Induced Residual Stresses and Cure Shrinkage in Micro-Scale Composite Structures with Different Constitutive Laws. *Appl. Compos. Mater.* **2018**, *25*, 67–84. [CrossRef]
27. Zhang, J.T.; Zhang, M.; Li, S.X.; Pavier, M.J.; Smith, D.J. Residual Stresses Created during Curing of a Polymer Matrix Composite Using a Viscoelastic Model. *Compos. Sci. Technol.* **2016**, *130*, 20–27. [CrossRef]
28. Arafath, A.R.A.; Vaziri, R.; Poursartip, A. Closed-Form Solution for Process-Induced Stresses and Deformation of a Composite Part Cured on a Solid Tool: Part I—Flat Geometries. *Compos. Part A Appl. Sci. Manuf.* **2008**, *39*, 1106–1117. [CrossRef]
29. Chen, W.; Zhang, D. A Micromechanics-Based Processing Model for Predicting Residual Stress in Fiber-Reinforced Polymer Matrix Composites. *Compos. Struct.* **2018**, *204*, 153–166. [CrossRef]
30. Courtois, A.; Marcin, L.; Benavente, M.; Ruiz, E.; Lévesque, M. Numerical Multiscale Homogenization Approach for Linearly Viscoelastic 3D Interlock Woven Composites. *Int. J. Solids Struct.* **2019**, *163*, 61–74. [CrossRef]
31. Vasylevskyi, K.; Tsukrov, I.; Drach, B.; Buntrock, H.; Gross, T. Identification of Process-Induced Residual Stresses in 3D Woven Carbon/Epoxy Composites by Combination of FEA and Blind Hole Drilling. *Compos. Part A Appl. Sci. Manuf.* **2020**, *130*, 105734. [CrossRef]
32. Liu, P.F.; Li, X.K. A Large-Scale Finite Element Model on Micromechanical Damage and Failure of Carbon Fiber/Epoxy Composites Including Thermal Residual Stress. *Appl. Compos. Mater.* **2018**, *25*, 545–560. [CrossRef]
33. Bloomfield, M.W.; Diaconu, C.G.; Weaver, P.M. On Feasible Regions of Lamination Parameters for Lay-up Optimization of Laminated Composites. *Proc. R. Soc. A Math. Phys. Eng. Sci.* **2008**, *465*, 1123–1143. [CrossRef]
34. Lian, J.; Xu, Z.; Ruan, X. Analysis and Control of Cured Deformation of Fiber-Reinforced Thermosetting Composites: A Review. *J. Zhejiang Univ.-Sci. A* **2019**, *20*, 311–333. [CrossRef]
35. Fu, Y.; Gao, X.; Yao, X. Mesoscopic Simulation on Curing Deformation and Residual Stresses of 3D Braided Composites. *Compos. Struct.* **2020**, *246*, 112387. [CrossRef]
36. Magnus Svanberg, J.; Anders Holmberg, J. Prediction of Shape Distortions Part I. FE-Implementation of a Path Dependent Constitutive Model. *Compos. Part A Appl. Sci. Manuf.* **2004**, *35*, 711–721. [CrossRef]
37. Ding, A.; Li, S.; Sun, J.; Wang, J.; Zu, L. A Thermo-Viscoelastic Model of Process-Induced Residual Stresses in Composite Structures with Considering Thermal Dependence. *Compos. Struct.* **2016**, *136*, 34–43. [CrossRef]
38. Liu, X.; Guan, Z.; Wang, X.; Jiang, T.; Geng, K.; Li, Z. Study on Cure-Induced Residual Stresses and Spring-in Deformation of L-Shaped Composite Laminates Using a Simplified Constitutive Model Considering Stress Relaxation. *Compos. Struct.* **2021**, *272*, 114203. [CrossRef]
39. Albert, C.; Fernlund, G. Spring-in and Warpage of Angled Composite Laminates. *Compos. Sci. Technol.* **2002**, *62*, 1895–1912. [CrossRef]

40. Shokrieh, M.M.; Safarabadi, M. *Understanding Residual Stresses in Polymer Matrix Composites*; Elsevier: Amsterdam, The Netherlands, 2021; ISBN 978-0-12-818817-0.
41. Wang, Y.; Mertiny, P. Mechanical and Thermal Properties of Epoxy Resin upon Addition of Low-Viscosity Modifier. *Polymers* **2024**, *16*, 2403. [CrossRef]
42. Rothenhäusler, F.; Ruckdaeschel, H. L-Arginine as a Bio-Based Curing Agent for Epoxy Resins: Glass Transition Temperature, Rheology and Latency. *Polymers* **2022**, *14*, 4331. [CrossRef]
43. Gorbatkina, Y.A.; Ivanova-Mumjieva, V.G.; Lebedeva, O.V. Adhesion of Modified Polymers to Fibres: Maxima on Adhesive Strength-Modifier Amount Curves and the Causes of Their Appearance. *Int. J. Adhes. Adhes.* **2009**, *29*, 9–17. [CrossRef]